

Imaging Spatial-Helical Mode Interference of Single Photons

E.J. Galvez, E. Johnson, B.J. Reschovsky, L.E. Coyle, and A. Shah

Department of Physics and Astronomy, Colgate University, 13 Oak Drive, Hamilton, New York 13346, U.S.A.

ABSTRACT

We present a study of the imaging of the interference of spatial-helical modes of single photons. This work includes a mathematical treatment that accounts for the direction of propagation and spatial mode degrees of freedom in the situation where light travels through an interferometer that prepares the light in distinct spatial modes and makes them interfere. We present results of the interference at the single photon level of the spatial-helical modes with topological charge 1 and 0. The results are consistent with the expectation that each photon carries the entire spatial mode information.

Keywords: Photons, Spatial Modes, Orbital Angular Momentum, Quantum Interference

1. INTRODUCTION

Interest in the manipulation of quantum information using light has brought attention to the spatial modes of light.¹ In particular, modes that are eigenstates of orbital angular momentum are suited as eigenstates for quantum information purposes. Features of quantum mechanics such as superposition and entanglement allow an expanded role for imaging, where the information is encoded in a quantum mechanical way, which may involve more than one particle (photon), and which go beyond the classical forms studied until now. As a first step toward this goal, in this study we report on the interference of orbital modes at the single-photon level by sending heralded photons through an interferometer that creates a superposition of different spatial modes.

The spatial-helical mode of photons has been used for purpose of entanglement with its topological charge as a mode-defining quantity. Although these spatial properties have been implicit in these studies, there has not been many studies imaging the photons themselves to demonstrate their modal properties. Previous imaging studies have devoted to other aspects of photons bearing orbital angular momentum, such as multimode Hong-Ou-Mandel interference,² correlations in spontaneous parametric down-conversion,³ and mode rotations due to Gouy phase.⁴

The spatial-helical mode has very interesting classical-wave properties shown in Fig. 1. It is a mode consisting of waves out of phase, with their phase varying as a function of the angular coordinate. The mode contains a phase singularity in its axis, a vortex, where phase is undefined, and around which the wave as a whole carries orbital angular momentum. Yet the quantum mechanical expectation is that the experimental result based on this well characterized classical object should remain the same as the light intensity is reduced all the way down to the single-photon level. How do we view the photons involved in these experiments? As part of answering this question the goal of this work is to show that the expected experimental results are indeed true.

Since the phase of singly-ringed spatial modes with a finite topological charge varies with the transverse angular coordinate, then the interference pattern between those modes and a fundamental Gaussian mode produces a pattern that is easily recognized. The amplitude of the interference pattern varies with the angular coordinate, and such pattern rotates as the phase between the component modes is changed.^{5,6} The simplest experiment of this type in the one we present in this article: imaging the superposition of modes with $\ell = 1$ and $\ell = 0$ and then change the phase in between the two modes. We do so by preparing the light in a single-photon state, send it through an interferometer that puts the light in a superposition of those modes, and scan a single-photon detector so as to take a picture one pixel at a time.

Further author information: (Send correspondence to E.J.G.)
E.J.G.: E-mail: egalvez@colgate.edu, Telephone: 1 315 228 7205

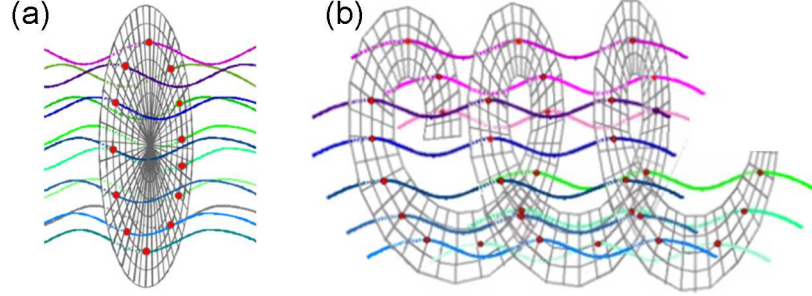


Figure 1. Classical view of light that carries a helical mode with a topological charge $\ell = 1$. It consists of a pattern where (a) the light waves in a transverse plane have a phase that increases with the transverse angular coordinate, or equivalently, (b) a mode where the points of equal phase (i.e., the wavefront) form helical surfaces of pitch equal to the wavelength of the light.

This article is divided the following way. In Sec. 2 we discuss a theoretical description that models the experiments. In this treatment the direction of propagation and spatial modes are evolved via unitary operations as the light goes through the components of the experimental apparatus. In Sec. 3 we present the experimental method and imaging results. We finish in Sec. 4 with conclusions and discussion.

2. THEORETICAL TREATMENT

The interferometer that we model is shown in Fig. 2. It consists of a Mach-Zehnder interferometer that has in general a diffractive optical element (DOE) in each arm. Each DOE puts the light in a particular spatial mode that is an orbital angular momentum eigenstate. We will devote the next section to the experimental details, so at this point it suffices to say that single photons enter the interferometer and their spatial probability density is imaged. As such each photon emerging from the interferometer is in a superposition of two spatial modes. The interferometer has symmetric non-polarizing beam splitters. The phase between the two modes is varied by changing the path-length difference between the two arms. The beam splitters and mirrors change the direction of propagation of the light to orthogonal directions. A useful model accounts for the changes in the direction of propagation in terms of orthogonal eigenstates of propagation directions: $|X\rangle$ and $|Y\rangle$, which represent light traveling along orthogonal coordinate axes labeled X and Y , respectively (see Fig. 2).^{7,8} We account for the transverse spatial mode via $|u_\ell\rangle = |u_\ell(r, \phi)\rangle$, where

$$u_\ell(r, \phi) = R(r, \ell)e^{i\ell\phi} \quad (1)$$

is a singly-ringed Laguerre-Gauss eigenstate,⁹ with

$$R(r, \ell) = \frac{2^{(|\ell|+1)/2} r^{|\ell|}}{\sqrt{\pi} w^{|\ell|+1}} e^{-r^2/w^2} \quad (2)$$

where ℓ is the topological charge and w is the $1/e$ -radius. (For simplicity we ignore the radius of curvature of the wavefront and the Gouy phase term.) A generic state is then expressed by $|d\rangle|u_\ell\rangle$, where $|d\rangle$, the direction of propagation state, is a linear combination of $|X\rangle$ and $|Y\rangle$.

The initial state is $|\psi_i\rangle = |X\rangle|u_0\rangle$, i.e., the photon is traveling along the X -direction in the fundamental spatial mode with $\ell = 0$. In accounting for the action of the interferometer we use a matrix approach to manipulate the direction of propagation eigenstates.⁸ Thus,

$$|X\rangle = \begin{pmatrix} 1 \\ 0 \end{pmatrix} \quad (3)$$

and

$$|Y\rangle = \begin{pmatrix} 0 \\ 1 \end{pmatrix}, \quad (4)$$

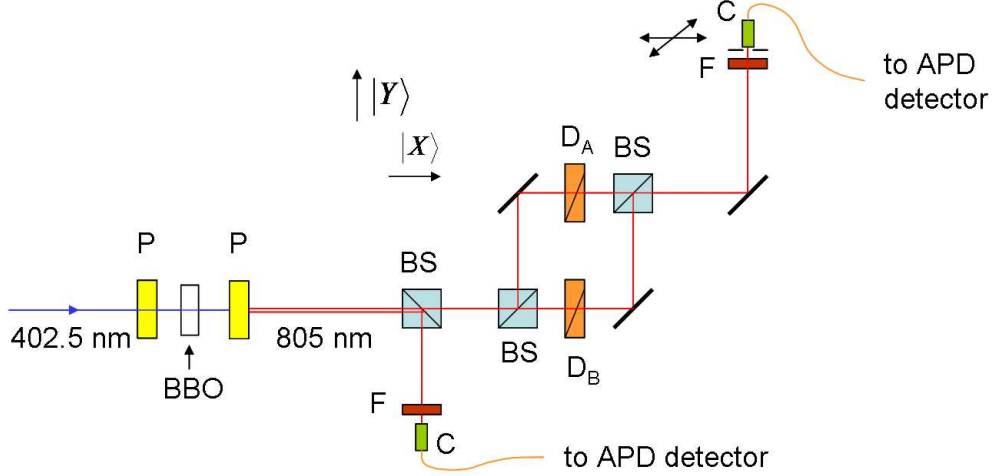


Figure 2. Schematic of the apparatus to study spatial mode interference of single photons. Components include down-conversion crystal (BBO), non-polarizing beam splitters (BS), polarizers (P), bandpass filters (F), diffractive optical elements (D), optical fiber collimator (C), and avalanche photodiode (APD). The state of the light with propagation direction along the two orthogonal directions is represented by $|X\rangle$ and $|Y\rangle$.

The beam splitter and mirror of the interferometer are then represented by

$$\hat{B} = \frac{1}{\sqrt{2}} \begin{pmatrix} \hat{I} & i\hat{\Pi} \\ i\hat{\Pi} & \hat{I} \end{pmatrix}, \quad (5)$$

and

$$\hat{M} = \begin{pmatrix} 0 & \hat{\Pi} \\ \hat{\Pi} & 0 \end{pmatrix}, \quad (6)$$

where \hat{I} and $\hat{\Pi}$ are the identity and parity operators, respectively, which operate on the spatial-mode substate:

$$\hat{I}|u_\ell(r, \phi)\rangle = |u_\ell(r, \phi)\rangle \quad (7)$$

and

$$\hat{\Pi}|u_\ell(r, \phi)\rangle = |u_\ell(r, -\phi)\rangle, \quad (8)$$

with the latter performing a mirror inversion (we will take the origin of the angular coordinate to be the vertical axis). The interferometer phases for light going through arms A and B are incorporated via the operator:

$$\hat{A} = \begin{pmatrix} e^{i\delta_A}\hat{I} & 0 \\ 0 & e^{i\delta_B}\hat{I} \end{pmatrix}, \quad (9)$$

where $\delta_A = 2\pi l_A/\lambda$ and $\delta_B = 2\pi l_B/\lambda$, with l_A and l_B being the lengths of the interferometer arms, and λ the wavelength of the light. The DOE's in each arm are represented by

$$\hat{D} = \begin{pmatrix} \hat{D}_A & 0 \\ 0 & \hat{D}_B \end{pmatrix}, \quad (10)$$

such that $\hat{D}_A|u_0\rangle = |u_A\rangle$ and $\hat{D}_B|u_0\rangle = |u_B\rangle$. That is, the DOE's put the input light in the mode with $\ell = 0$ going through arms A and B into modes with $\ell = \ell_A$ and $\ell = \ell_B$, respectively.

The interferometer operator then becomes

$$\hat{Z} = \hat{B}\hat{A}\hat{D}\hat{M}\hat{B}, \quad (11)$$

which upon replacement of the individual matrices we get

$$\hat{Z} = \frac{1}{2} \begin{pmatrix} ie^{i\delta_A} \hat{D}_A + ie^{i\delta_B} \hat{D}_B & e^{i\delta_A} \hat{D}_A \hat{\Pi} - e^{i\delta_B} \hat{D}_B \hat{\Pi} \\ -e^{i\delta_A} \hat{\Pi} \hat{D}_A + e^{i\delta_B} \hat{\Pi} \hat{D}_B & ie^{i\delta_A} \hat{\Pi} \hat{D}_A \hat{\Pi} + ie^{i\delta_B} \hat{\Pi} \hat{D}_B \hat{\Pi} \end{pmatrix}, \quad (12)$$

where we have used $\hat{\Pi}^2 = \hat{I}$. Detection of the light leaving the interferometer along the X -direction involves the corresponding projector

$$\hat{P}_X = \begin{pmatrix} \hat{I} & 0 \\ 0 & 0 \end{pmatrix}. \quad (13)$$

The probability amplitude density of detecting a photon at location (r, ϕ) in the transverse plane is

$$p = \langle r, \phi | \hat{\Pi} \hat{P}_X \hat{Z} | X \rangle | u_0 \rangle \quad (14)$$

$$= \frac{i}{2} e^{i\delta_B} (R_A e^{i\delta - \ell_A \phi} + R_B e^{-i\ell_B \phi}), \quad (15)$$

where we have used the shorthand notation: $R_A = R(r, \ell_A)$ and $R_B = R(r, \ell_B)$ and $\delta = \delta_A - \delta_B$. The added term $\hat{\Pi}$ accounts for the mirror reflection after the interferometer (see Fig. 2). The probability density of detecting a photon is given by

$$P_p = |p|^2 = \frac{1}{4} (R_A^2 + R_B^2 + 2R_A R_B \cos[\delta - (\ell_A - \ell_B)\phi]). \quad (16)$$

The probability density has the same form of the classical interference of two different spatial modes, which consists of a pattern that rotates about the origin when δ is varied.^{5,6}

For example, for the case when $\ell_A = 1$ and $\ell_B = 0$, as is the case for the experiment described below, the pattern for different values of δ is shown in Fig. 3. It can be seen that it is an off center probability distribution that rotates about a central point as a function of δ . This type of pattern is well known in the interference of classical beams (see for example Ref. 10). This modal interference pattern exhibits an off-center phase singularity. The case for $\delta = 0$ is shown in the figure, where the phase information has been encoded in the gray scale. As the phase is varied the singularity also rotates with the pattern.

3. EXPERIMENTS

We prepared the light in a non-classical state by generating photon pairs via type-I spontaneous parametric down conversion. The apparatus is shown in Fig. 2. A diode laser beam of wavelength 402.5 nm and power 50 mW was sent to a 3-mm thick beta-barium-borate nonlinear crystal, producing collinear degenerate pairs of photons at a wavelength of 805 nm. A Glan-Thompson polarizer with transmission axis horizontal was placed before the crystal to make sure the polarization of the light incident to the crystal was horizontal. A second polarizer with transmission axis vertical placed after the crystal eliminated the part of the pump beam that did not produce

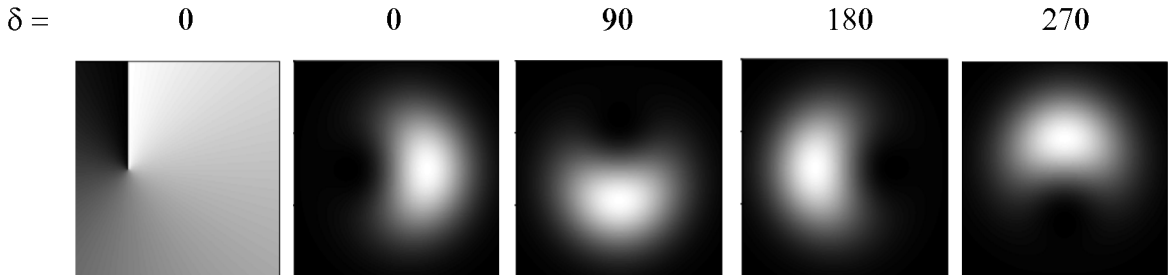


Figure 3. Simulation of the mode of the light when the interferometer puts it in a superposition of $\ell = 1$ and $\ell = 0$ modes. The left-most frame shows a contour map of the phase of the probability amplitude distribution encoded in a gray scale for $\delta = 0$. The adjacent four frames show the probability density (i.e., Eq. 16) for different relative phases δ (in degrees) between the two modes.

pairs and any other light coming from the laser. The latter polarizer transmitted the down-converted photons, which were vertically polarized. A non-polarizing 50-50 beam splitter separated the photon pairs half the time, with a heralding photon going directly to be detected while the other one (i.e., the heralded one) going through the interferometer before being detected. By detecting the two photons in coincidence we effectively projected the state of the light onto a single-photon state.¹¹

The heralding photon passed through a 10-nm band-pass filter and was coupled into a multimode fiber that sent it to an avalanche photo diode (APD) single-photon detector. The heralded photon went through a Mach-Zehnder interferometer, as shown in Fig. 2. Arm *A* of the interferometer had a commercial spiral phase plate made of polymer deposited onto a glass blank.¹² The angular ramp had a discontinuous step equivalent to a free-space path length of 807.5 nm, which is about one full wavelength of the down-converted light. Thus, the spiral phase plate imparted a topological charge $\ell_A = 1$ to the transmitted light. In the far field this beam was approximately in a Laguerre-Gauss eigenstate with azimuthal index $\ell = 1$ and radial index $p = 0$ (i.e., singly ringed).⁹ It has been shown that the transmitted mode is in a superposition of same- ℓ but different- p eigenstates.¹³ A more accurate analytical description of the resulting mode has been derived,¹⁴ but to a good approximation the detected light is in the $\ell = 1$ eigenstate. Arm *B* had just a glass blank of the same thickness and material as the substrate of the spiral phase plate. Thus, it did not change the $\ell = 0$ mode of the incoming light.

The output of the interferometer was allowed to expand by letting the light travel a distance of about 1 m after the interferometer and before being collected by a fiber collimator coupled to a multimode optical fiber. The collimator was preceded by an iris, and together were translated in a two dimensional plane by stepper-motor-driven linear stages coupled by gear reduction mechanical elements.

We took scans of the iris-collimator in a square grid that was contained in a plane transverse to the propagation direction of the heralded photons. The diameter of the iris was set to about 0.5 mm. A detection event constituted a collapse of the photon wavefunction onto the transmitted area of the iris. Photons recorded by the APD, with an efficiency of about 60% (nominal), generated pulses sent to coincidence electronics.

Figure 4 shows a sequence of experimental scans for different values of the interferometer phase δ . In each scan the iris-collimator were moved together in steps of 0.22 mm in a transverse plane. The set of points in a scan formed a 40×40 grid of data imaging the probability density of the heralded photon. Each point displays the coincidence counts accumulated over 5 s. The images are contour graphs with steps of 50 counts, as shown in the scale on the right side of the figure. The phase of each scan was set by adjusting the tilt of the glass blank in arm *B*. Because of the time it took to position the iris-collimator in between data points, each scan took

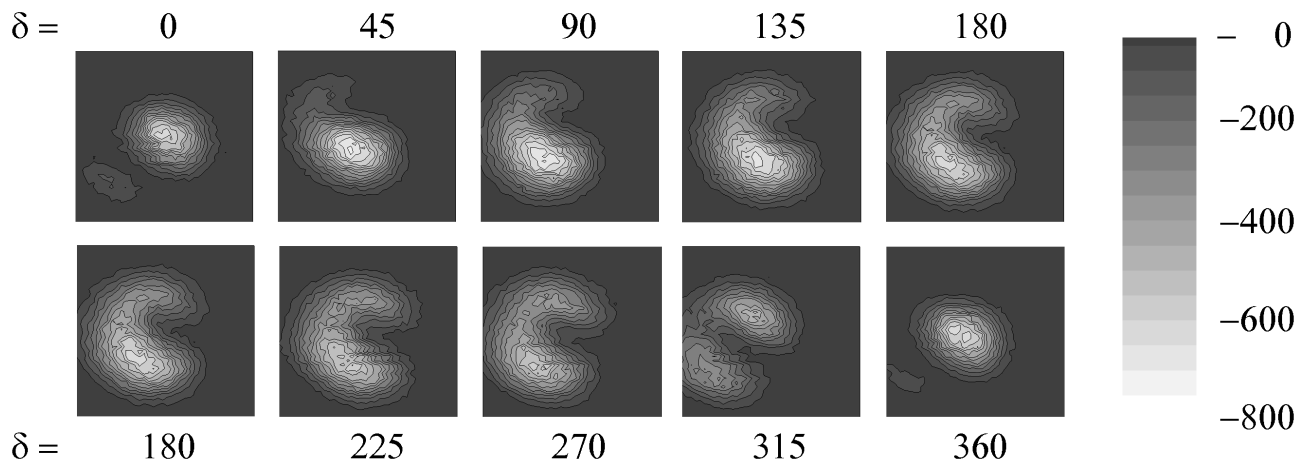


Figure 4. Measurements of the probability density of a single photon in a superposition of $\ell = 1$ and $\ell = 0$ modes taken by recording the heralded photon counts as the detector aperture was scanned in a two-dimensional transverse plane. The frames were taken consecutively for increasing values of the relative phase between the modes δ (in degrees).

about four hours to record. Thus, the entire sequence of nine scans required that the interferometer remained phase-stable for a span of 36 hours, with round-the-clock data taking. To accomplish this the interferometer was shielded from vibrations and air currents.

The sequence of images show a consistent progression. First, the frames for $\delta = 0$ and $\delta = 360^\circ$ are remarkably similar, which points to the consistency of the data. Then the pattern progresses smoothly from $\delta = 45^\circ$ to $\delta = 315^\circ$, consistent with a pattern revolving about a central point, which is the main prediction of the theory. However, the pattern evolved faster than our phase step between $\delta = 0$ and $\delta = 45^\circ$, and between $\delta = 315^\circ$ and $\delta = 360^\circ$. Such a nonlinear transition could be due to a lack of alignment or the lack of symmetry in the profile of the input pump beam from the diode laser. A lack of alignment seemed a less likely reason because numerous attempts at realignment did not change the pattern. We imaged the pump beam and indeed confirmed that its spatial mode was non-Gaussian. An irregular distribution is likely to explain the observed evolution as a function of the phase, although we did not do a detailed modeling of this. However, we believe that these data supports the theoretical expectation—that single photons are interfering with themselves in a superposition of $\ell = 1$ and $\ell = 0$ modes. We are in the process of implementing a pump beam from a gas laser with pure Gaussian profile that would produce results of better quality.

4. CONCLUSIONS AND DISCUSSION

In summary, we present measurements of the probability distribution of single photons in a superposition of two spatial modes. The imaged pattern had an off-center helical wavefront, which is the result of the superposition of $\ell = 1$ and $\ell = 0$ modes. The results show strong evidence of single-photon modal interference: the imaged pattern shifted around a central spot completing one period for a 2π phase difference between the two modes. The pattern did not rotate evenly with the phase, as expected from Fig. 3, but we attribute this to the non-Gaussian profile of the input beam emitted by the diode laser pump.

That the interference at the single-photon level is the same as the classical many-photon pattern implies that light in a spatial-helical mode has to be composed of photons carrying the entire mode information. Thus, imaging the interference of spatial modes of single photons suggests a view that the “size” of the photon extends in a transverse dimension by the size of the spatial mode and in a longitudinal dimension by its coherence length.

An interesting extension of these experiments constitute the imaging of the modal interference of biphotons. This is the case where both photons from down-conversion enter the interferometer together. The interesting aspect of biphotons is that they are linked via quantum mechanics, and so the component photons behave as one. The detection of two photons after the interferometer leads to interesting non-classical effects because these photons may be traveling in disparate directions after the interferometer and yet carry a common image information.

ACKNOWLEDGMENTS

We thank K. Wilson for his contributions in the early stages of this project. This work was supported by a grant from Research Corporation and National Science Foundation grant DUE-042882.

REFERENCES

1. Molina-Terriza, G., Torres, J.P., and Torner, L., “Twisted photons,” *Nature Phys.* **3**, 305-310 (2007).
2. Walborn, S.P., de Oliveira, A.N., Thebaldi, R.S., and Monken, C.H., “Entanglement and conservation of orbital angular momentum in spontaneous parametric down conversion,” *Phys. Rev. A* **69**, 023811 1-6 (2004).
3. Altman, A.R., Köprülü, K.G., Corndorf, E., Kumar, P., and Barbosa, G.A., “Quantum imaging of nonlocal spatial correlations induced by orbital angular momentum,” *Phys. Rev. Lett.* **94**, 123601 1-4 (2005).
4. Kawase, D., Miyamoto, Y., Takeda, M., Sasaki, K., and Takeuchi, S., “Observing quantum correlation of photons in Laguerre-Gauss modes using the Gouy phase,” *Phys. Rev. Lett.* **101**, 0505010 1-4 (2008).
5. Galvez, E.J., Smiley, N., and Fernandes, N., “Composite optical vortices formed by collinear Laguerre-Gauss beams,” *Proc. SPIE* **6131**, 19–26 (2006).

6. Baumann, S.M., Kalb, D.M., MacMillan, L.H., and Galvez, E.J., "Propagation dynamics of optical vortices due to Gouy phase," *Opt. Express* **17**, 9818-9827 (2009).
7. Gadway, B.R., Galvez, E.J., and DeZela, F. , "Bell-Inequality violations with single photons in momentum and polarization," *J. Phys. B* **42**, 015503 1-9 (2009)
8. Galvez, E.J., "Qubit quantum mechanics with correlated-photon experiments," *Am. J. Phys.* (in press).
9. Allen, L., Beijersbergen, M.W., Spreeuw, R.J.C., and Woerdman, J.P., "Orbital angular momentum of light and the transformation of Laguerre-Gauss modes," *Phys. Rev. A* **92**, 8185-8189 (1992).
10. Galvez, E.J., Crawford, P.R., Sztul, H.I., Pysher, M.J., Haglin, P.J., and Williams, R.E., "Geometric phase associated with mode transformations of optical beams bearing orbital angular momentum," *Phys. Rev. Lett.* **90**, 201901 1-4, (2003).
11. U'Ren, A.B., Silberhorn, C., Ball, J.L., Banaszek, K., and Walmsley, I.A., "Characterization of the non-classical nature of conditionally prepared single photons," *Phys. Rev. A* **72**, 021802 1-4 (2005).
12. RPC Photonics Inc.
13. Beijersbergen, M.W., Coerwinkel, R.P.C., Kristensen, M., and Woerdman, J.P., "Helical-wavefront laser beams produced with a spiral phase plate," *Opt. Commun.* **112**, 321-324 (1994).
14. Berry, M.V., "Optical vortices evolving from helicoidal integer and fractional phase steps," *J. Opt. A* **6**, 259-268 (2004).